Template-Synthesized Hierarchical Porous Carbon Nanocages for High Rate Performance Supercapacitors

Liang Jiang[1,*], Jing Wang[2,*], Huali Zhang[3], Suzhen Zhang[4], Xuyan Mao[1], Lihua Xing[2], Xiangyu Xu[1], Jie Yang[1], Shifeng Hou[1]

[1] Bio-Nano & Medical Engineering Institute, Jining Medical University, 133 Hehua Road, Jining, 272067, China.
[2] Department of Physics and Information Engineering, Jining University, 1 Xingtan Road, Qufu, 273155, China.
[3] Collaborative Innovation Center, Jining Medical University, 133 Hehua Road, Jining, 272067, China.
[4] Department of Hematology, Affiliated Hospital of Jining Medical University, 89 Guhuai Road, Jining, 272029, China.
[*]E-mail: jiangliangjnmc@126.com (Liang Jiang), wangjingouc@126.com (Jing Wang).

Carbon nanocages with a hierarchical structure have attracted increasing attention in recent years due to the high rate capability of supercapacitors based on such materials. In this study, cubic carbon nanocages (CNCs) with a hierarchical porous structure were prepared by using cubic magnesium oxide as a template and sucrose as the carbon source. The carbon nanocages interconnect to form 3D nanoparticles, when used as the electrode material for supercapacitors, exhibit a high specific capacitance and excellent rate capability. The specific capacitance at a current density of 50 A g^{-1} can reach 135 F g^{-1}. The excellent capacitive performance of carbon nanocages is attributed to the macropores formed by the cavity inside the cages and interparticle voids, which provide a fast pathway for ion transportation by shortening the diffusion pathway for electrolyte ions. Moreover, CNCs possess good cycling stability with a capacitance retention of 96.2% after 10000 cycles.

1. INTRODUCTION

With the increasing environmental crisis, developing high performance and environment-friendly energy storage technology has become an urgent task. Supercapacitors have been widely used in high-power supply equipment, military equipment and smart grids because of their high power density, long cycle life and fast charging ability[1, 2]. Carbon-based supercapacitors have become the most widely used devices due to their high specific surface area, excellent electrical conductivity and chemical

stability. Various carbon materials have been investigated as electrode materials in electrical double layer capacitors (EDLCs), including activated carbons, mesoporous carbons, carbon nanotubes (CNTs), graphene and so on[3-5]. However, the tortuous micropore structure of activated carbon results in great resistance to the transmission of electrolyte ions and exhibits a poor rate capability. A mesoporous structure is not as good as a microporous structure for charge storage[6, 7].

Therefore, the porous structure of carbon materials has an important effect on their capacitive performance. Micropores can improve the storage capacity of electrolyte ions; macropores can be used as a reservoir for electrolyte ions, which shortens the diffusion pathway of electrolyte ions; and mesopores can reduce the diffusion resistance for electrolyte ions[8, 9]. The synergistic effect of hierarchical porous carbons with micropores, mesopores and macropores exhibits an excellent capacitive performance[10, 11]. It should be noted that the development of novel hierarchical porous carbon has become a research hotspot in the field of supercapacitor electrode materials.

Carbon nanocages have attracted much interest because of their hierarchical porous structure[12-15]. The stacking of such nanocages leads to the formation of a 3-dimension (3D) nanoarchitecture. The 3D nanostructures can provide a continuous electron pathway to ensure high electrical conductivity. The cavity inside the cages and interparticle voids can be used as ion-buffering reservoirs. The existence of such macropores ensures fast ion diffusion via a shortening of diffusion pathways, shortens the diffusion pathway of electrolyte ions, and improves the rate capability of the electrode material. There features indicate that carbon nanocages are a potential electrode material for supercapacitors and exhibit high capacitance and an excellent rate capability. The commonly used methods for preparing carbon nanocages are chemical vapor deposition and active metal reduction, which are complex and involve a high cost[12, 14, 16]. Development of a simple and economical method to synthesize high performance carbon nanocage electrode materials is an important topic at present.

In this work, carbon nanocages were prepared using the cubic structure of magnesium oxide formed by metal magnesium combustion as a template and sucrose as a carbon source. After high temperature carbonization, carbon nanocages were obtained after removal of the magnesium oxide template. The prepared material had a hierarchical porous structure and exhibited a high specific capacitance and good rate performance.

2. EXPERIMENTAL

2.1. Preparation of porous carbon

A magnesium ribbon was ignited in air. The obtained magnesium oxide was ground into powder. Then, 1 g sucrose and 2 g magnesium oxide powder were dissolved in 6 g water. The mixture was dried at 80 °C for 24 h. Pyrolysis was performed in a N_2 atmosphere at varying temperatures for 2 h. The sample was immersed in a dilute hydrochloric acid solution at 80 °C for 8 h to remove the MgO template and washed to neutral with deionized water. Finally, the sample was dried at 60 °C in an oven and denoted as CNCX, where X is the carbonization temperature.

2.2. Physicochemical characterization

Scanning electron microscopy (SEM) images of the sample morphology were recorded using a microscope (Zeiss ultra plus) at 3 kV; transmission electron microscopy (TEM) characterization was carried out using a microscope (JEM-2000EX, JOE) operated at 120 kV and (FEI tecnai G2) at 200 kV. Powder X-ray diffraction (XRD) measurements were carried out using an XRD-6100 (Shimadzu). The Quantachrome AutoSorb iQ system was used to measure the specific surface area and pore size distribution. The specific surface area was calculated by a conventional Brunauer–Emmet–Teller (BET) plot. X-ray photoelectron spectroscopy (XPS) experiments were performed using a Thermo Scientific spectrometer with an Escalab 250 Xi X-ray as the excitation source.

2.3. Electrochemical test

Carbon, acetylene black and polytetrafluoroethylene (PTFE) were used according to a mass ratio of 85:10:5 and ground and mixed evenly. The mixture presented a clay state following the addition of a small amount of ethanol. A circular electrode membrane with a diameter of 9 mm was sandwiched between two nickel foams and used as the current collector. The electrochemical performance of the samples was evaluated in a three electrode cell device, with the prepared sample membrane, a Pt plate and Ag/AgCl electrode used as the working electrode, counter electrode and reference electrode, respectively. In the two-electrode system, two working electrodes were placed on both sides of polypropylene with polypropylene as the membrane and then sealed with a 2032 battery after adding a steel sheet. The electrolyte used in the electrochemical tests was a 6 M KOH solution. Cyclic voltammetry (CV) and electrochemical impedance spectroscopy (EIS) tests were performed using an electrochemical workstation (Shanghai CH Instruments, CHI760E) in a three-electrode system. Galvanostatic charge-discharge tests were carried out using a battery test station (BTS; Neware, China) with a symmetric electrode configuration.

The specific capacitance can be calculated from the following formula according to the charge and discharge data:

$$C = \frac{4i\Delta t}{\Delta V m}$$

where m, ΔV, I and Δt are the total mass of the active material on the two electrodes, voltage drop, discharge current and discharge time, respectively.

The formula used for calculating the virtual capacitance of the electrode materials by impedance spectroscopy is as follows:

$$C'' = \frac{Z'}{2\pi f m (|Z'|^2 + |Z''|^2)}$$

where Z', Z'', f and m are the real part of the electrode resistance, imaginary part of the electrode resistance, operating frequency and mass of the active material, respectively[17].

3. RESULTS AND DISCUSSION

Fig. 1a shows that the magnesium oxide template has a cubic structure with a size range of 100-200 nm. The morphologies of CNC800 were observed from SEM and TEM images, as shown in Fig. 1b and Fig. 1c. The SEM image of CNC800 shows that 3D nanoparticles formed by the stacking of a large number of tiny cubic particles with a size range of 100-200 nm. The size of the hollow in the cage is exactly the same as that of magnesium oxide. The shell thickness of the nanocages is typically less than 5 nm, as shown in Fig. 1d. Magnesium oxide is used as a hard template in the process of carbonization, and a carbon layer can be formed on the template by high temperature carbonization of sucrose. With the removal of magnesium oxide, a hollow cage structure appears.
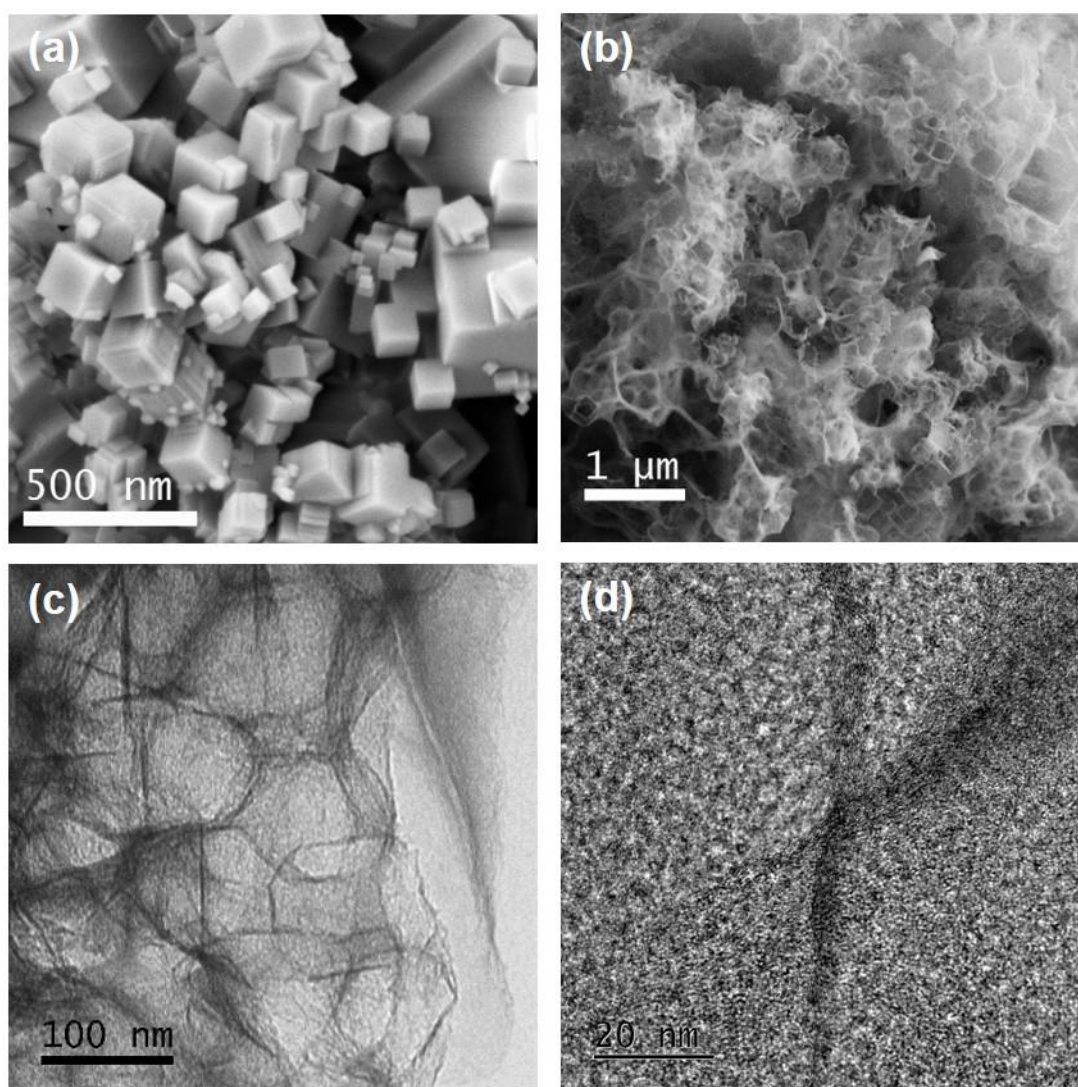
Figure 1. SEM images of magnesium oxide (a) and CNC800 (b); TEM images of CNC800 (c, d).

XRD was used to characterize the crystal structure of the carbon nanocages, as shown in Fig. 2a. Broad diffraction peaks can be observed at an angle of approximately 24°, which corresponds to the (002)

plane of the graphite structure. With the increasing carbonization temperature, the crystal structure of the carbon materials changes. For CNC900, the diffraction peaks for the (100) plane are observed at 43°, which shows that the graphitization degree of CNC900 is obviously improved. The results indicate the amorphous characteristics for the partially graphitized structure of the CNCs.
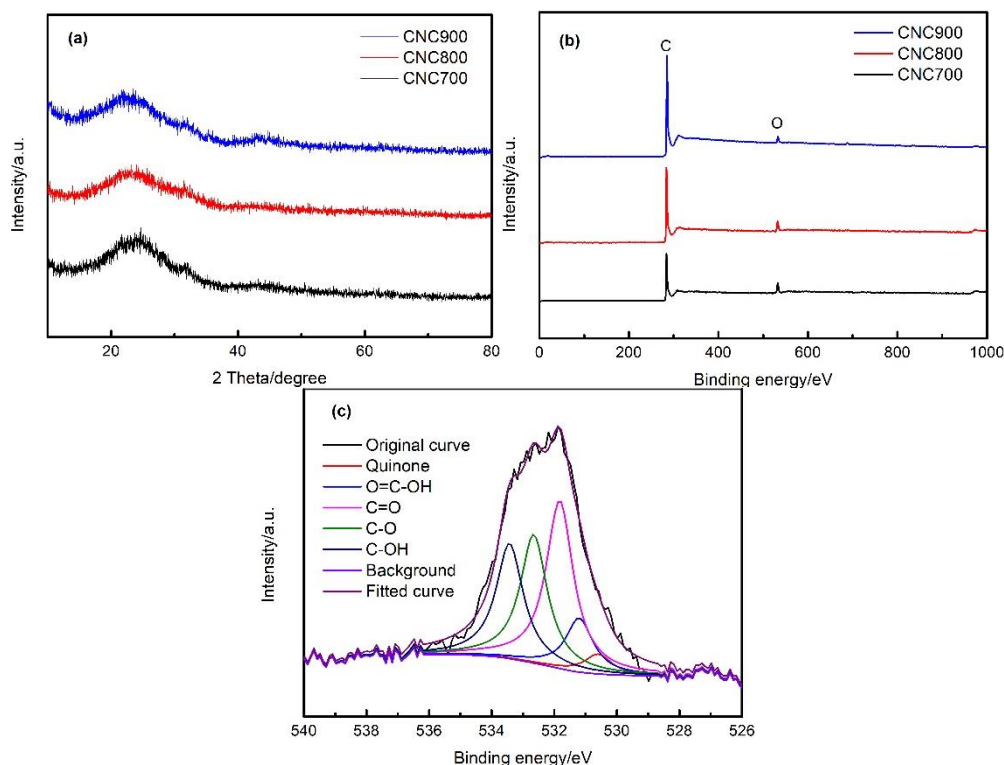
Figure 2. XRD patterns of the CNCs (a); XPS spectra of the CNCs (b); high resolution O_{1s} peaks of CNC800 (c).

XPS measurements were carried out to evaluate the chemical composition on the surface. As shown in Fig. 2b, the surface of the carbon materials mainly contains two elements: carbon and oxygen. With increasing carbonization temperature, the atomic percentage of oxygen on the surface of the carbon nanocages is 10.4%, 6.0% and 3.8%. The high resolution O1s peaks for CNC800 are fitted into five components originating from the oxygen in the quinone groups (530.4 eV) and oxygen in -COOH (531.2 eV), -C=O (531.9 eV), -C-O (532.8 eV), and -OH (533.4 eV), as shown in Fig. 2c[18, 19]. In general, oxygen-containing functional groups on the surface of the carbon material can improve the wettability of the electrolyte solution and hence the accessible surface area for enhancing the electrical double layer[14, 15]. Therefore, the capacitive performance of CNCs will be improved. Studies have indicated that the oxygen in carboxyl and phenolic groups is more conducive to the formation of an electric double layer on the surface of carbon materials in an alkaline electrolyte[18, 20]. The content of oxygen in the phenolic and carboxyl groups is 34.8%; these oxygen functional groups enhance the capacitance of carbon materials.
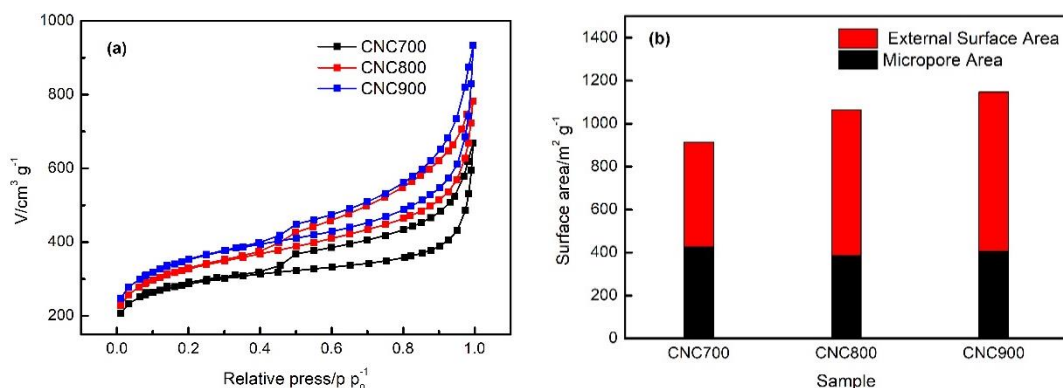
Figure 3. N$_2$ adsorption–desorption isotherm and surface area of the CNCs (a); micropore and external surface area of the CNCs (b).

The specific surface area and porous structure of the carbon materials were characterized by nitrogen adsorption-desorption measurements. As shown in Fig. 3a, the N$_2$ adsorption-desorption curves of the CNCs belong to type-IV isotherms (based on the IUPAC classification). The hysteresis loop appears at a relative pressure of 0.5, indicating that a large number of mesoporous structures exist in the carbon materials. The specific surface areas of CNC700, CNC800 and CNC900 are 914, 1065 and 1147 m^2 g^{-1}, respectively. As the carbonization temperature increases, the specific surface area gradually increases, possibly due to the activation of magnesium oxide at high temperature. Microporous structure parameters are obtained by the t-plot method. As shown in Fig. 3b, compared with CNC700, the proportion of the micropore area in CNC800 and CNC900 significantly decreased. This decrease in micropore area indicates that there are a large number of mesoporous channels in CNC800 and CNC900. Moreover, the sharp jump in the curve at higher relative pressures of 0.9-1 suggests the existence of macropores in the CNCs[13]. The nitrogen adsorption experiment shows that the carbon nanocages prepared by using magnesium oxide as the template have a hierarchical structure, which is beneficial to shorten the diffusion pathways of ions.

Cyclic voltammetry (CV) measurements were used to investigate the capacitive performance of the nanocage materials by using a three-electrode system in a 6.0 M KOH aqueous electrolyte. Fig. 4a shows the CV curves for the CNCs measured at a scan rate of 10 mV s^{-1}. The curve presented with nearly symmetrical rectangular shapes, implying that the capacitive response mainly arises from the electrochemical double layer capacitance. In addition, broad reversible humps can be observed for CNC700 and CNC800 due to the pseudo-capacitance that occurs via redox reactions[15]. Compared with CNC900, CNC700 and CNC800 have a higher response current, and the response current is proportional to the capacitance value. Although CNC900 has the highest specific surface area, the specific surface area is not the only factor that determines the capacitance. The graphitization degree of the carbon materials will affect the wettability of the electrolyte solution. The high graphitization degree of CNC900 reduces the wettability between electrolyte and carbon materials. In addition, with the increasing carbonization temperature, the oxygen-containing functional groups on the surface of the carbon materials gradually decrease. Oxygen-containing functional groups can produce a pseudocapacitance through a reversible oxidation-reduction reaction in an alkaline electrolyte [18, 21, 22]. Oxygen-containing functional groups can also improve the hydrophilicity of the surface of carbon

materials. Therefore, CNC700 and CNC800 have a higher specific capacitance. It is noted that as the scan rates increased to 1000 mV s^{-1}, the CV curve for the CNC700 electrode became spindle-shaped and those for CNC800 and CNC900 still had rectangular-shapes without an oblique angle, indicating the highly capacitive nature and rate capability of carbon nanocages carbonized at high temperature.
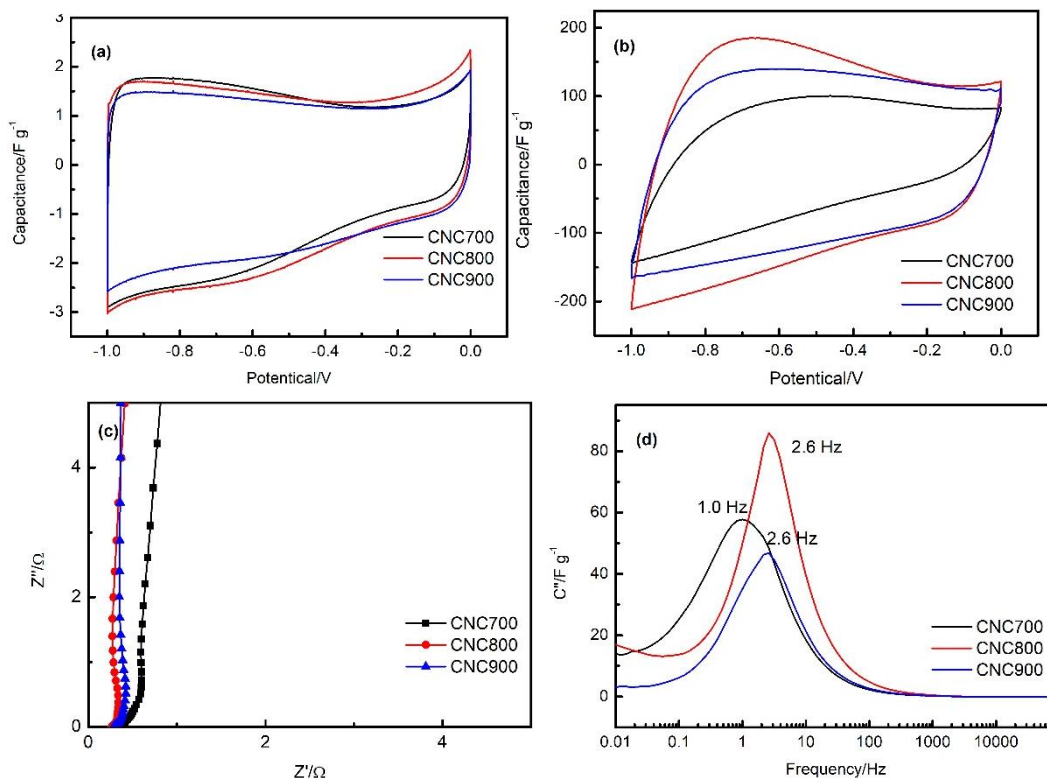
Figure 4. CV curves for the CNCs measured at a scan rate of 10 mV s^{-1}(a); 1000 mV s^{-1} (b); Nyquist plot for the CNCs (c); changes in the imaginary part of the capacitance with frequency for the CNCs (d).

Electrochemical impedance spectroscopy was used to further study the capacitive characteristics of the electrode materials. Nyquist plots are shown in Fig. 4c. The intercept of the plot in the high-frequency region represents the equivalent series resistance, which includes the intrinsic resistance of the carbon material, electrolyte resistance, and contact resistance of the current collector/electrode interface[23]. The values of the intersection for CNC700, CNC800 and CNC900 are 0.34, 0.27, and 0.28 Ω, respectively. At an intermediate frequency, the curve does not appear to be a semicircle, indicating fast ion diffusion of the porous electrode material. The EIS curve for the CNC sample is perpendicular to the real axis in the low-frequency region, which is similar to the characteristic of the ideal capacitive behavior.
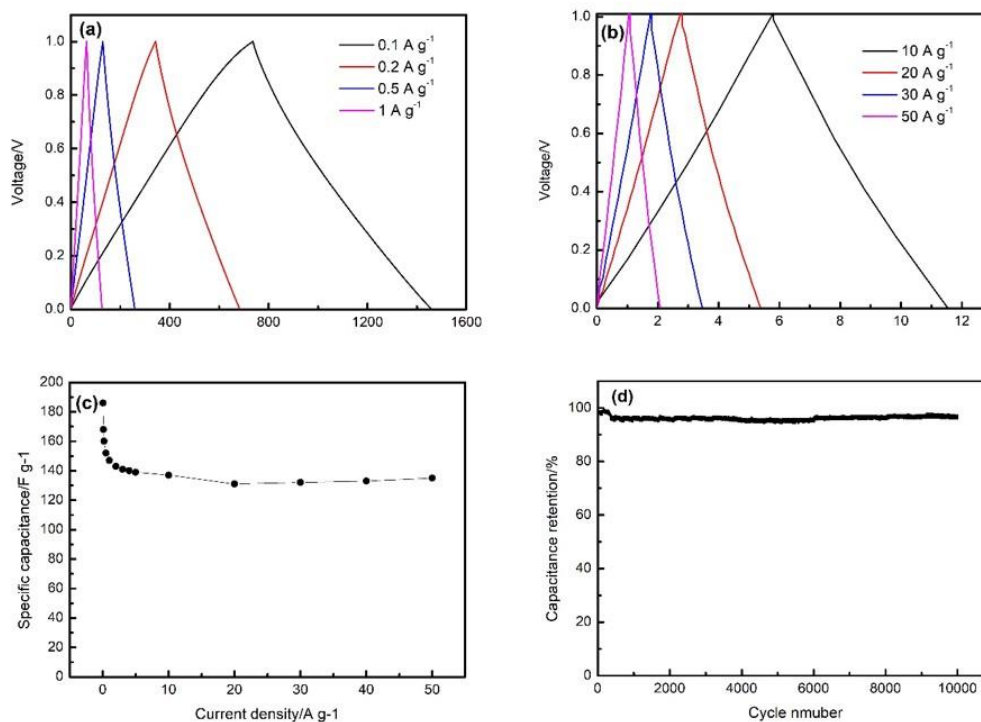
Figure 5. Galvanostatic charge-discharge curves for CNC800 at varying current densities of CNC800 (a, b); specific capacitance at varying current densities (c); cycling stability tests at a current density of 10 A g^{-1} for CNC800 (d).

EIS data were processed to obtain the imaginary part of the capacitance to further investigate the electrolyte ion transport inside the porous electrode, as shown in Fig. 4d. A peak can be observed with a changing frequency, which is considered to be the demarcation point for the electrode resistance behavior and capacitance behavior[17]. The reciprocal of the frequency at the peak is the time constant t_0, which is the minimum time required to discharge the energy of a device with an efficiency of more than 50%. The time constant for the CNCs can be analyzed from Fig. 4d. The CNC800 and CNC900 electrodes exhibit a faster frequency response than CNC700, indicating that the carbon nanocage structure is conducive to the rapid transmission of electrolyte ions and electrons at a high current. The CV and EIS measurements show that CNC800 is an ideal electrode material for supercapacitors because of its high specific capacitance and excellent rate performance.

A galvanostatic charge-discharge test for CNC800 was carried out in the two-electrode system. Fig. 5 shows the charge-discharge curve for CNC800 at varying current densities. The galvanostatic charge-discharge curves present nearly symmetrical triangles with a slight deviation, which proves that the capacitance arises from both double-layer capacitance and pseudocapacitance. At a current density of 10 A g^{-1}, there is still no obvious IR drop, indicating that the electrode material has a very small equivalent series resistance.

The specific capacitance at different current densities is shown in Fig. 5c. At a current density of 0.05 A g^{-1}, the specific capacitance of the CNC800 reaches 193 F g^{-1} and the area-normalized capacitance reaches 22.1 μF cm^{-2}, which exceeds the theoretical specific capacitance of a clean graphite surface[24].

The presence of oxygen-containing functional groups on the surface increases the hydrophilicity of CNCs and increases the ion accessible specific surface area for electrolyte ions. In addition, pseudocapacitance will be generated through faradic reactions in the alkaline electrolyte. The synergistic effect of the above factors leads to an increase in the area-normalized capacitance. At a high current density of 50 A g^{-1}, the specific capacitance can still reach 135 F g^{-1} and the capacitance retention rate can reach 70.0%, showing excellent rate performance. As shown in Tab.1, the results were compared with hierarchical porous carbons reported in the literature. CNC800 exhibited a better capacitive performance than other hierarchical porous carbons. The good capacitive performance of the CNC material can be attributed to its hierarchical porous structure. First, macropores composed of a cavity inside a cage with interparticle voids acting as a reservoir for electrolyte ions lead to a shortening of the pathway for electrolyte ion migration into the micropores and the mesopores, resulting in the easier transfer of ions at a high current. Second, mesopores are considered to be transport channels for electrolyte ions, reducing the charge transfer resistance. Finally, the synergistic effect of macropores and mesopores provides an efficient transport path for ion transport.

Table 1. Comparison of the CNC800 prepared in this work with materials in the literature

Sample	Capacitance (F g^{-1})	Current density (A g^{-1})	Electrolyte	Ref
CNC800	135	50	6 M KOH	This work
OPC	84	15	6 M KOH	[25]
N-PCNs	118	10	6 M KOH	[26]
AC3-700	98	1	6 M KOH	[27]
HPNC950	70	10	6 M KOH	[28]
BAC-2	63	10	6 M KOH	[29]
NGC700	84	10	6 M KOH	[30]

The cycling stability of the sample was evaluated by galvanostatic charge-discharge cycles of 10 A g^{-1} in a two-electrode system. The capacitance retention curve is shown in Fig. 5d. The capacitance retention curve slightly decreases in the first 500 cycles, but subsequently tends to show a stable capacitance. After 10000 cycles, the retention rate of the capacitance is 96.2%, suggesting excellent cyclic stability.

4. CONCLUSION

In this work, carbon nanocages with a hierarchical pore structure were prepared by using cubic magnesium oxide as a template and sucrose as the carbon source. CNCs have a small intrinsic resistance and low charge transfer resistance. The synergistic effect of a macroporous and mesoporous structure reduces the transmission resistance of electrolyte ions. The existence of macropores and voids in the cage structure reduces the distance travelled by electrolyte ions entering the pore and improves the

transmission performance of electrolyte ions at a high current. The above results prove that carbon nanocages are a potential electrode material for supercapacitors.

References

1. Y. G. Wang, Y. F. Song and Y. Y. Xia, *Chem. Soc. Rev.*, 45 (2016) 5925.
2. X. L. Chen, R. Paul and L. M. Dai, *Natl. Sci. Rev,* 4 (2017) 453.
3. M. Inagaki, H. Konno and O. Tanaike, *J. Power Sources*, 195 (2010) 7880.
4. X. Li and B. Q. Wei, *Nano Energy*, 2 (2013) 159.
5. F. M. Zeng, Z. Li, X. Y. Li, J. Wang, Z. Kong, Y. C. Sun, Z. J. Liu and H. B. Feng, *Appl. Surf. Sci.*, 467 (2019) 229.
6. C. Largeot, C. Portet, J. Chmiola, P. L. Taberna, Y. Gogotsi and P. Simon, *J. Am. Chem. Soc.*, 130 (2008) 2730.
7. J. Huang, B. G. Sumpter and V. Meunier, *Chemistry - A European Journal* 14 (2008) 6614.
8. D. W. Wang, F. Li, M. Liu, G. Q. Lu and H. M. Cheng, *Angew. Chem. Int. Ed.*, 47 (2008) 373.
9. L. Dong, Z. X. Chen, D. Yang and H. B. Lu, *Rsc Advances*, 3 (2013) 21183.
10. D. Hu, C. Y. Chen and Q. Liu, *J. Mater. Sci.*, 53 (2018) 12310.
11. S. Dutta, A. Bhaumik and K. C. W. Wu, *Energ. Environ. Sci.*, 7 (2014) 3574.
12. K. Xie, X. T. Qin, X. Z. Wang, Y. N. Wang, H. S. Tao, Q. Wu, L. J. Yang and Z. Hu, *Adv. Mater.*, 24 (2012) 347.
13. J. Zhao, H. W. Lai, Z. Y. Lyu, Y. F. Jiang, K. Xie, X. Z. Wang, Q. Wu, L. J. Yang, Z. Jin, Y. W. Ma, J. Liu and Z. Hu, *Adv. Mater.*, 27 (2015) 3541.
14. L. Jiang, J. Wang, X. Y. Mao, X. Y. Xu, B. Zhang, J. Yang, Y. F. Wang, J. Zhu and S. F. Hou, *Carbon,* 111 (2017) 207.
15. J. Q. Shao, M. Y. Song, G. Wu, Y. H. Zhou, J. F. Wan, X. Ren and F. W. Ma, *Energy Storage Materials*, 13 (2018) 57.
16. M. Qian, F. Xu, H. Bi, T. Q. Lin and F. Q. Huang, *Carbon,* 112 (2017) 47.
17. P. L. Taberna, P. Simon and J. F. Fauvarque, *J. Electrochem. Soc.*, 150 (2003) A292.
18. Y. J. Oh, J. J. Yoo, Y. I. Kim, J. K. Yoon, H. N. Yoon, J. H. Kim and S. B. Park, *Electrochim. Acta*, 116 (2014) 118.
19. C. M. Chen, Q. Zhang, X. C. Zhao, B. S. Zhang, Q. Q. Kong, M. G. Yang, Q. H. Yang, M. Z. Wang, Y. G. Yang, R. Schlöglb and D. S. Su, *J. Mater. Chem.,* 22 (2012) 14076.
20. Y. Fang, B. Luo, Y. Y. Jia, X. L. Li, B. Wang, Y. Song, F. Y. Kang and L. J. Zhi, *Adv. Mater.*, 24 (2012) 6348.
21. J. Y. Liang, T. T. Qu, X. Kun, Y. Zhang, S. Y. Chen, Y. C. Cao, M. J. Xie and X. F. Guo, *Appl. Surf. Sci.,* 436 (2018) 934.
22. C. G. Tang, Y. J. Liu, D. G. Yang, M. Yang and H. M. Li, *Carbon,* 122 (2017) 538.
23. H. Lu, K. S. Kim, Y. H. Kwon, X. M. Sun, R. Ryoo and X. S. Zhao, *J. Mater. Chem.* A., 6 (2018) 10388.

24. H. Shi, *Electrochim. Acta,* 41 (1996) 1633.
25. J. H. Xu, W. L. Zhang, D. X. Hou, W. M. Huang and H. B. Lin, *Chinese Chem. Lett*., 28 (2017) 2295.
26. G. X. Wang, L. Liu, L. L. Zhang, X. Y. Fu, M. Liu, Y. X. Zhang, Y. F. Yu and A. B. Chen, *J. Electron. Mater*., 47 (2018) 5816.
27. A. J. Li, X. Y. Chuan, Y. Yang, X. Cao, D. B. Huang and Z. Q. Yang, *Electrochemistry,* 85 (2017) 708.
28. Y. M. Wang, T. Liu, X. J. Lin, H. Chen, S. Chen, Z. J. Jiang, Y. Chen, J. Liu, J. L. Huang and M. L. Liu, *Acs. Sustain. Chem. Eng.,* 6 (2018) 13932.
29. E. Lei, W. Li, C. H. Ma, Z. Xu and S. X. Liu, *Appl. Surf. Sci.*, 457 (2018) 477.
30. H. W. Mi, X. D. Yang, J. Hu, Q. L. Zhang and J. H. Liu, *Front. Chem.*, 6 (2018).